Antiviral Research 158 (2018) 226–237

Contents lists available at ScienceDirect

Antiviral Research

journal homepage: www.elsevier.com/locate/antiviral

High-throughput drug screening using the Ebola virus transcription- and replication-competent virus-like particle system

Nakyung Lee[a,1], David Shum[a,1], Alexander König[b], Hichul Kim[a], Jinyeong Heo[a], Saehong Min[b], Jihye Lee[c], Yoonae Ko[d], Inhee Choi[d], Honggun Lee[e], Constantin Radu[e], Thomas Hoenen[f], Ji-Young Min[c,**], Marc P. Windisch[b,*]

[a] Assay Development & Screening, Institut Pasteur Korea, 16, Daewangpangyo-ro 712 Beon-gil, Bundang-gu, Seongnam-si, Gyeonggi-do, South Korea
[b] Applied Molecular Virology Laboratory, Institut Pasteur Korea, South Korea
[c] Respiratory Virus Research Laboratory, Institut Pasteur Korea, South Korea
[d] Bioinformatics, Institut Pasteur Korea, South Korea
[e] Automation and Logistics Management, Institut Pasteur Korea, South Korea
[f] Institute for Molecular Virology and Cell Biology, Friedrich-Loeffler-Institut, Greifswald-Insel Riems, Germany

ARTICLE INFO

Keywords:
Ebola virus
Hemorrhagic fever
Viral life cycle modeling system
Drug screening
FDA drugs
Repurposing

ABSTRACT

The massive epidemic of Ebola virus disease (EVD) in West Africa, followed in recent months by two outbreaks in the Democratic Republic of the Congo, underline the importance of this severe disease. Because Ebola virus (EBOV) must be manipulated under biosafety level 4 (BSL4) containment, the discovery and development of virus-specific therapies have been hampered. Recently, a transient transfection-based transcription- and replication competent virus-like particle (trVLP) system was described, enabling modeling of the entire EBOV life cycle under BSL2 conditions. Using this system, we optimized the condition for bulk co-transfection of multiple plasmids, developed a luciferase reporter-based assay in 384-well microtiter plates, and performed a high-throughput screening (HTS) campaign of an 8,354-compound collection consisting of U.S. Food & Drug Administration (FDA) -approved drugs, bioactives, kinase inhibitors, and natural products in duplicates. The HTS achieved a good signal-to-background ratio with a low percent coefficient of variation resulting in Z' = 0.7, and data points were reproducible with $R^2 = 0.89$, indicative of a robust assay. After applying stringent hit selection criteria of ≥70% EBOV trVLP inhibition and ≥70% cell viability, 381 hits were selected targeting early, entry, and replication steps and 49 hits targeting late, maturation, and secretion steps in the viral life cycle. Of the total 430 hits, 220 were confirmed by dose-response analysis in the primary HTS assay. They were subsequently triaged by time-of-addition assays, then clustered and ranked according to their chemical structures, biological functions, therapeutic index, and maximum inhibition. Several novel drugs have been identified to very efficiently inhibit EBOV. Interestingly, most showed pharmacological activity in treatments for central nervous system-related diseases. We developed and screened an HTS assay using the novel EBOV trVLP system. Newly identified inhibitors are useful tools to study the poorly understood EBOV life cycle. In addition, they also provide opportunities to either repurpose FDA-approved drugs or develop novel viral interventions to combat EVD.

1. Introduction

The 2014 Ebola virus (EBOV) outbreak was the most serious Ebola epidemic in recent history and was a major global threat to people and economies. The occurrence in recent months of two outbreaks in the Democratic Republic of the Congo underline the importance of this highly virulent virus. EBOV is a member of the *Filoviridae* family and is a filamentous, enveloped, negative-stranded RNA virus with a genome

Abbreviations: EBOV, Ebola virus; EVD, EBOV disease; VHF, Viral hemorrhagic fever; trVLP, transcription- and replication-competent virus-like particle; HTS, High-throughput screening; DRC, Dose-response curve; Imax, Maximum inhibition; GPCR, G-protein coupled receptors

* Corresponding author.
** Co-corresponding author. Current address. GSK, 14200 Shady Grove Road, Rockville, MD, 20850, USA.
E-mail addresses: ji-young.x.min@gsk.com (J.-Y. Min), marc.windisch@ip-korea.org (M.P. Windisch).
[1] These authors equally contributed to this work.

https://doi.org/10.1016/j.antiviral.2018.08.013
Received 25 June 2018; Received in revised form 16 August 2018; Accepted 20 August 2018
Available online 24 August 2018

size of 18–19 kb encoding 7 proteins. EBOV disease (EVD) has been neglected for decades; neither EBOV-specific therapies nor vaccines are available because major patient populations live in low-income countries. In addition, EBOV is a causative agent of a severe form of viral hemorrhagic fever (VHF) with fatality rates as high as 90%. Therefore, research must be conducted in biosafety level 4 (BSL4) containments, which are limited worldwide. To overcome this, surrogate systems including virus-like particle (VLP) and minigenome systems that can be used in BSL2 facilities have been developed to study EBOV entry and replication, respectively (Hoenen et al., 2006; Edwards et al., 2015; Basu et al., 2015; Anantpadma et al., 2016). These systems are limited to specific aspects of the virus life cycle. With the recent development of a transcription- and replication competent virus-like particle (trVLP) system for EBOV (Hoenen and Feldmann, 2014; Watt et al., 2014), it became possible to study almost all aspects of the viral life cycle by transferring cell culture supernatants from infected (transduced) target cells to naïve target cells (Fig. 1A). One hallmark of this system is that besides entry and replication, it possible to evaluate EBOV morphogenesis and budding in only one single HTS campaign under BSL2 conditions. Furthermore, the EBOV trVLP system follows a more authentic and physiologically relevant approach compared to other surrogate systems because it does not depend on components from other unrelated viruses. In addition, proteins crucial for EBOV particle morphogenesis, budding, and entry are not overexpressed. Therefore, the EBOV trVLP system is an ideal platform to study unexploited steps in the EBOV life cycle and provides a powerful tool to discover novel viral interventions. Recently, the trVLP was shown to be a useful tool to characterize and to evaluate inhibitors in small-scale approaches (Nelson et al., 2016, 2017; Dyall et al., 2018).

Here, we report on the development and application of a target-free high-throughput screening (HTS) assay utilizing the novel EBOV trVLP system, which was miniaturized into 384-well microtiter plate format enabling rapid testing of large compound libraries. The EBOV trVLP system was validated using the previously reported EBOV inhibitors tamoxifen and toremifene (Johansen et al., 2013; Kouznetsova et al., 2014). As a proof-of-concept, a small molecule collection containing U.S. Food & Drug Administration (FDA) -approved drugs, bioactives, kinase inhibitors, and investigational compounds was screened in duplicate to assess assay reproducibility and robustness. The identified compounds for entry and replication, morphogenesis, and budding were further confirmed by dose-response curve (DRC) analysis in the primary HTS assay, categorized according to their biological functions, and ranked according to their antiviral activities.

2. Material and methods

2.1. Cells and plasmids

The human embryonic kidney HEK293T cell line was grown at 37 °C in 5% CO_2. HEK293T cells were propagated in complete growth medium containing Dulbecco's minimum essential medium (DMEM) supplemented with 10% heat-inactivated fetal bovine serum (FBS), 100 Units/mL penicillin, and 100 g/mL streptomycin (P/S). All cell culture supplies were from Wellgene (Gyeongsan, Korea) and Invitrogen (Carlsbad, CA, USA). Plasmids for the EBOLA trVLP system (pCAGGS-NP, pCAGGS-VP35, pCAGGS-VP30, pCAGGS-L, p4cis-vRNA-RLuc, pCAGGS-T7, and pCAGGS-Tim1) were kindly provided by Dr. Thomas Hoenen (NIH/NIAID, Rocky Mountain Laboratories, Hamilton, MT, USA). Plasmids were amplified in DH5α competent cells (Intron Biotechnology, Seongnam, Korea) and extracted using EndoFree Plasmid Maxi Kit (Qiagen, Hilden, Germany) according to the manufacturer's specifications.

2.2. Production of EBOV trVLPs in p0 producer cells

HEK293T cells (10^7 in 20 mL) were seeded at into T175 flasks in complete growth media and incubated for 24 h. EBOV trVLP system plasmids were diluted from stocks in Opti-Mem (Gibco, Grand Island, NY, USA) with the following concentrations per T175 flask: pCAGGS-NP at 2.5 μg, pCAGGS-VP35 at 2.5 μg, pCAGGS-VP30 at 1.5 μg, pCAGGS-L at 20 μg, p4cis-vRNA-Rluc at 5 μg, and pCAGGS-T7 at 5 μg. The plasmids were combined to a total volume of 3.5 mL with 122 μL TransIT-LT1/T175 flask contents and incubated at room temperature for 15 min to promote complex formation. The transfection mixes were then gently added into T175 flasks. At 24 h post-transfection, the media was exchanged for 30 mL growth media with 5% FBS and 1% P/S and further incubated for an additional 48 h. All supernatants from p0 producer cells were collected followed by centrifugation at 2,000 rpm for 5 min and stored at −80 °C until use. Cells were lysed after supernatant transfer to quantify virus production followed by addition of 1 mL Renilla-Glo (Promega, Madison, WI, USA). Relative luciferase unit (RLU) activity was measured using Victor III (PerkinElmer, Waltham, MA, USA).

2.3. Generation of EBOV trVLP p1 and p2 target cells

EBOV trVLP system plasmids were diluted from stock in Opti-MEM with the following concentrations per well of a 384-well microtiter plate: pCAGGS-NP at 1.6 ng, pCAGGS-VP35 at 1.6 ng, pCAGGS-VP30 at 0.9 ng, pCAGGS-L at 12.5 ng, and pCAGGS-Tim1 at 3.1 ng. The plasmids were combined to a total volume of 10 μL with 62 nL TransIT-LT1/well and incubated at room temperature for 30 min to promote complex formation. The transfection mixes were dispensed (Wellmate, Thermo Fisher Scientific, Waltham, MA, USA) into 384-well microtiter plates followed by HEK293T suspensions at 6000 cells/well in 20 μL complete growth media containing 8 μg/mL polybrene. After the reverse transfection procedure, the assay plates containing p1 and p2 target cells were incubated for 24 h until use.

2.4. Compound libraries

The library used for the screen combines 8354 small molecules obtained from commercial sources including: Spectrum Collection (MicroSource Discovery Systems, Gaylordsville, CT, USA), Prestwick Chemical Library (Prestwick Chemical, Illkirch, France), LOPAC®1,280 (Sigma-Aldrich, St. Louis, MO, USA), Tocriscreen compound Library (Tocris Bioscience, Bristol, UK), Anti-cancer & Kinase Inhibitor Library (Selleck Chemicals, Houston, TX, USA), and NIH Clinical Collection (Baltimore, MD, USA). The collection contains structurally diverse compounds from known drugs, experimental bioactives, kinase inhibitors, and pure natural products. These compounds target several therapeutic areas including oncology, infections, neuropsychiatry, cardiology, and immunology. All compounds were dissolved at a concentration of 10 mM in 100% dimethyl sulfoxide (DMSO, v/v) and formatted into 384-well polypropylene plates for storage at 20 °C.

2.5. Screening of compound libraries with the EBOV trVLP system

To measure EBOV entry and replication, p1 target cells were seeded as previously described, and 1 μL compounds were transferred (Apricot Personal Pipettor, Apricot Design, Covina, CA, USA) from the compound library into an intermediate 384-well polypropylene plate. The compounds were mixed with 19 μL DMEM media, and 5 μL/well was transferred into 384-well assay plates and incubated with p1 cells for 2 h. Next, 15 μL EBOV trVLPs harvested from p0 producer cells were added and spin inoculated at 1000 rpm for 8 min. The plates were incubated for 72 h in a 37 °C incubator. All compounds were screened at a final test concentration of 10 μM in 0.5% DMSO (v/v). To determine EBOV secretion, p2 cells were seeded as described, and 20 μL cell culture supernatants were transferred from compound-treated p1 cells to p2 cells and spin inoculated at 1,000 rpm for 8 min. The assay plates were incubated for 72 h in a 37 °C incubator. To measure luciferase

reporter activity after 72 h, assay plates with p1 and p2 cells were transferred into the Cell Explorer automated robotic platform (PerkinElmer). Assay plates were equilibrated to room temperature, and 10 µL Renilla-Glo was added to each well with a bulk reagent dispenser (Multidrop, Thermo Fisher Scientific). After 10 min incubation, RLUs were measured using EnVision (PerkinElmer).

2.6. Determination of cell viability

To determine cell viability in the presence of compounds, HEK293T cells were seeded at 6000 cells/well in 45 µL complete growth media into 384-well assay plates and treated with 5 µL serially diluted compounds and incubated for 72 h. Cells were fixed with 10 µL paraformaldehyde at a final concentration of 2% (w/v) and stained with 5 µM Hoechst, followed by imaging using Opera (PerkinElmer).

2.7. Statistical evaluation of assays and compounds

To evaluate the quality of assay for HTS, the signal-to-background ratio (S/B) and the Z′-factor were determined using the following formulas (Zhang et al., 1999): S/B = mean signal/mean background, Z′ factor = $1 - ([3\sigma_{c+} + 3\sigma_{c-}]/[|\mu_{c+} - \mu_{c-}|])$. S/B ratio is a simple measurement to assess signal window between positive control and background signal. Z′ factor is used in HTS/HCS to evaluate the performance of the assay and access the data variation. Z' factor values are $0 < Z < 0.5$ that means signal window is small and $0.5 \leq Z < 1$ representing signal window is large and "high-quality" HTS assay. To find drug candidates from dose-response curve (DRC) analysis, Therapeutic index (TI) was determined using the formulas: TI = ratio of half maximal effective concentration (EC_{50})/half-maximal cytotoxicity concentration (CC_{50}).

2.8. Hit confirmation by dose-response curve analysis

For dose-response curve (DRC) analysis, hits were supplied from internal library stocks and transferred into intermediate 384-well polypropylene plates. Compounds were analyzed by 10-point serial doubling dilution, with final concentrations of 50, 25, 12, 6, 3, 1.5, 0.8, 0.4, 0.2, and 0.1 µM (Apricot Personal Pipettor), and 5 µL volume of compounds were transferred into the assay plates. Reporter activity using luminescence readout and cell viability with imaging was performed as previously described.

2.9. Hit clustering and categorization

Confirmed hits were clustered based on scaffold analysis (Bemis and Murcko, 1996), which defines the union of rings plus linker atoms connections using Vortex (Dotmatics, Bishop's Stortford, UK). To cluster the hits targeting early and late steps in the EBOV life cycle, we first generated a Bemis-Murcko scaffold of each compound using Vortex (Dotmatics) and grouped according to scaffold similarity. Next, the clustered molecules were reviewed to assess whether the structural groups were well defined within the respective scaffold. We combined information on the pharmacological actions of each compound from vendors and the ChemIDPlus database (National Library of Medicine, 2017), MESH database (National Library of Medicine, 2017), SciFinder (Chemical Abstract Services, 2017). All pharmacological actions including minor and major classifications were accounted for since known drugs and bioactives are reported to treat various diseases. Information on drug approval status was taken from the DrugBank database (Law et al., 2014).

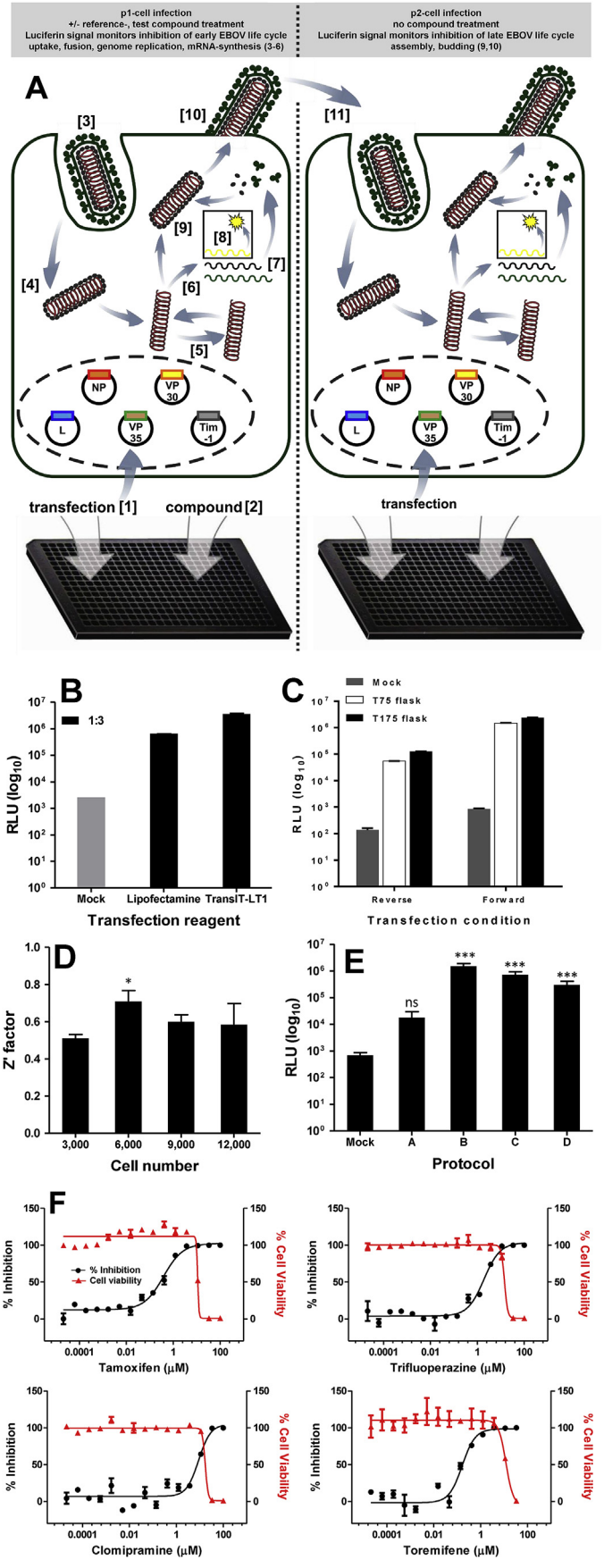

(Caption on next page)

Fig. 1. EBOV trVLP HTS assay development. (A) EBOV life cycle modeling system. Reporter activity of p1 cells was assessed to measure the inhibition of viral entry, replication, and transcription (viral early steps). Supernatants of p1 cells were transferred to p2 to monitor assembly and secretion (viral late steps). (B) Transfection reagent and plasmid ratio optimization in p0 producer cells generating EBOV trVLPs. Transfection without EBOV 4-cis minigenome (Mock). (C) Optimization of bulk EBOV trVLP production in T75 and T175 flasks using the reverse versus forward transfection method. Transfection without EBOV 4-cis minigenome (Mock). (D) Validation of cell density in 384-well microtiter plates at 3,000, 6,000, 9,000, and 12,000 cells/well. The Z′ factor was calculated at 0.5% DMSO (v/v) and non-infected cells. Statistical significance between 3,000 and 6,000 conditions was analyzed by Student's *t*-test (ns, not significant, $^{*}p < 0.05$, $^{**}p < 0.01$, $^{***}p < 0.001$). (E) Transfection optimization in 384-well microtiter plates for p1 and p2 cell generation. Statistical significance between control (non-infected cells, Mock) and Protocols A, B, C, D as analyzed by Student's *t*-test (ns, not significant, $^{*}p < 0.05$, $^{**}p < 0.01$, $^{***}p < 0.001$). (F) Activity of reference compounds in p1 cells. DRC analysis of tamoxifen, trifluoperazine, clomipramine, and toremifene. Compound concentration, EBOV trVLP inhibition in percent, and cell viability in percent are depicted on the x-, left y- (black), and right y-axis (red), respectively.

3. Results

3.1. Strategy and development of an EBOV trVLP HTS assay

Taking advantage of the recently described EBOV trVLP system, we implemented a strategy to develop an HTS assay in 384-well plate format (Hoenen and Feldmann, 2014). Briefly, the EBOV trVLP system is based on the transient transfection of 6 plasmids expressing viral proteins and a minigenome that is initially artificially T7 RNA polymerase driven. Sufficient amounts of EBOV trVLPs are produced upon transfection of HEK293T cells (producer cells, p0). Cell culture supernatants are harvested and transferred to target HEK293T cells (p1) that are transiently transfected with factors crucial for viral entry, replication, and particle morphogenesis (Fig. 1A). By transferring cell culture supernatants from infected (transduced) p1 cells to p2 cells, the entire EBOV life cycle can be targeted under authentic conditions. This trans-complementation strategy is key to safely handling EBOV in BSL2 containment.

To identify the most efficient and convenient way of transient transfection of multiple plasmids, we first tested several conditions for bulk co-transfection of the 6 plasmids towards large-scale EBOV trVLP production in p0 cells. Two different transfection reagents were tested side-by-side with 1:3 ratios of plasmid to reagent mix based on the published approach in 6-well plates (Fig. 1B) (Watt et al., 2014). The resulting transfection efficiency of EBOV trVLP from p0 producer cells was assessed by measuring luciferase activity. Comparing the two reagents, transfection with TransIT-LT1 resulted in up to 10-fold greater reporter activity compared to Lipofectamine 2000. Therefore, TransIT-LT1 was selected for further transfection experiments with a plasmid to reagent ratio of 1:3 to enable maximum complex formation for 6 plasmids. To produce sufficient EBOV trVLPs for HTS, we systematically tested bulk forward and reverse transfection in T75 and T175 flasks. Reverse transfection was performed by incubating plasmid mixtures and cell suspensions before seeding; whereas cells were seeded 24 h prior to transfection in forward transfection. A luminescence comparison between the two processes showed that forward transfection yielded a > 20-fold higher transfection efficiency than reverse transfection independent of flask size (Fig. 1C). Therefore, EBOV trVLPs production in T175 flasks was selected due to a larger EBOV trVLP yield in the supernatant volume.

Next, to establish infection conditions in 384-well plate format, we evaluated the efficiency of EBOV trVLPs under varying cell seeding densities of 3,000, 6,000, 9,000, and 12,000 cells/well (Fig. 1D). Z′ factors were calculated by comparing luciferase activities of infected cells treated with 0.5% DMSO (v/v) and non-infected cells. The results showed that 6000 cells/well achieved the best overall performance as measured by the Z' factor of 0.7 and the highest overall infection efficiency based on RLU readout.

Using these infection and cell-seeding conditions, we next focused on the optimization of p1 cells in 384-well plates by testing different transfection conditions. Several methods shown in Table 1 were tested, including pre-mixture of cells with transfection reagents plus plasmids, reverse transfection with plasmid complex followed by cell seeding, and forward transfection with cell seeding followed by plasmid complex addition at various time points (Fig. 1E). As a direct comparison, the same batch of p0 EBOV trVLPs was used in this experiment. Method B using reverse transfection with complex formation yielded the highest infection rate with an average of 1.5×10^6 RLUs.

In summary, we evaluated the sequential steps of the assay: 1) transfection conditions for bulk production of trVLPs in p0 cells in flasks, 2) infectivity of p0 produced trVLPs in p1 cells under different seeding conditions in 384-well microtiter plates, and 3) infectivity of p0 produced trVLPs in p1 cells under different cell transfection conditions to establish the EBOV trVLP p1 system in 384-well microtiter plates. As a proof-of-concept, we evaluated the inhibitory activities of tamoxifen, trifluoperazine, clomipramine, and toremifene, which were previously described to inhibit EBOV trVLP infection (Fig. 1F) (Johansen et al., 2013; Kouznetsova et al., 2014). Inhibitory activity was assessed in p1 cells using luminescence readout, and the half maximal effective concentration (EC_{50}) values of compounds were calculated. Based on the antiviral activity observed by EC_{50} and maximum inhibition in percent (Imax (%)) (Table 2), we selected tamoxifen and toremifene as reference drugs for our EBOV trVLP HTS. For HTS assay quality and analysis, toremifene at 10 μM was used as a positive control, because of reproducible 100% inhibition without cytotoxicity through the independent experiments. We optimized co-transfection and cell plating conditions to generate p0 producer and p1 cells, selected reference compounds, and produced sufficient amounts of EBOV trVLP for the HTS campaign.

3.2. EBOV trVLP HTS assay automation

As the next step toward HTS with the EBOV trVLP system, the assay was adapted for automated liquid handling of cell seeding, reagent dispensing, compound treatment, and supernatant transfer from p1 into p2 target cells. First, we compared manual and automated dispensing of 25 μL luciferase reagent. RLUs were in the range of 3.8×10^6 using a manual pipettor; however, automated dispensing resulted in a ~88-fold reduction due to bubbling from the lysis buffer containing detergent, which interfered with the overall RLU signal (Fig. 2A). Consequently, the automated dispensing volume was adjusted to 10 μL to minimize the overall agitation, and this resulted in RLUs similar to the

Table 1
Transfection optimization protocols in 384-well microtiter plates.

Protocol #	Methods	
A	Pre-mixture transfection	1) Prepare cells and DNA mixture separately 2) Mix them and add to 384-well plates
B	Reverse transfection	1) Add DNA mixture to 384-well plates 2) After 30 min, seed cells on plates
C	Forward transfection	1) Seed cells in 384-well plates 2) After 30 min, add DNA mixture to plates
D	Forward transfection	1) Seed cells in 384-well plates 2) After 24 h, add DNA mixture to plates

Table 2
DRC analysis of tamoxifen, trifluoperazine, clomipramine, and toremifene in p1 cells.

	Tamoxifen	Trifluoperazine	Clomipramine	Toremifene
EC_{50} (μM)	0.38 ± 0.07	1.90 ± 0.17	9.08 ± 0.59	0.16 ± 0.03
CC_{50} (μM)	11.02 ± 0.05	14.35 ± 0.11	17.08 ± 0.93	11.80 ± 0.35
Imax (%)	100	100	100	100
TI	29	8	2	74

EC_{50}: half maximal effective concentration, CC_{50}: half-maximal cytotoxicity concentration, maximum inhibition: Imax (%), therapeutic index (TI). EC_{50} and CC_{50} values represent mean ± standard deviations (SD) from 4 independent experiments.

Table 3
Optimization of supernatant transfer assay.

	Target cells	Z′	S/B	%CV
w/o spin inoculation	p1	0.45	98	18
	p2	−0.56	7	38
with spin inoculation	p1	0.58	296	14
	p2	0.62	105	12

Z′ factor calculated using 0.5% DMSO (v/v) and 10 μM toremifene. S/B: signal-to-background ratio: %CV, coefficient of variation.

manual process at a reduced reagent cost per well.

To assess the impact of compounds on the entire EBOV life cycle, we employed a supernatant transfer strategy in which cell culture supernatants were transferred from p1 to naïve p2 cells. The supernatant transfer process was evaluated using the following criteria of acceptance: uniform supernatant transfer, minimal cell monolayer disturbance during the transfer process, low well-to-well variation across an entire 384-well microtiter plate, and high infectivity between EBOV trVLPs released in p1 into p2 cells. Various supernatant volumes were tested using the liquid transfer station, and we selected a 20 μL supernatant transfer that resulted in overall uniformity between wells and no disturbance of the cell monolayer. To measure RLUs, p1 cells were treated with 0.5% DMSO (v/v) and toremifene at 10 μM in 0.5% DMSO (v/v) for 2 h followed by supernatant transfer to p2 cells (Fig. 2B). The signal-to-background ratio (S/B) between DMSO- and toremifene-treated cells was approximately 100-fold in p1 cells; however, after supernatant transfer, the window was reduced to 7-fold in p2 cells. To

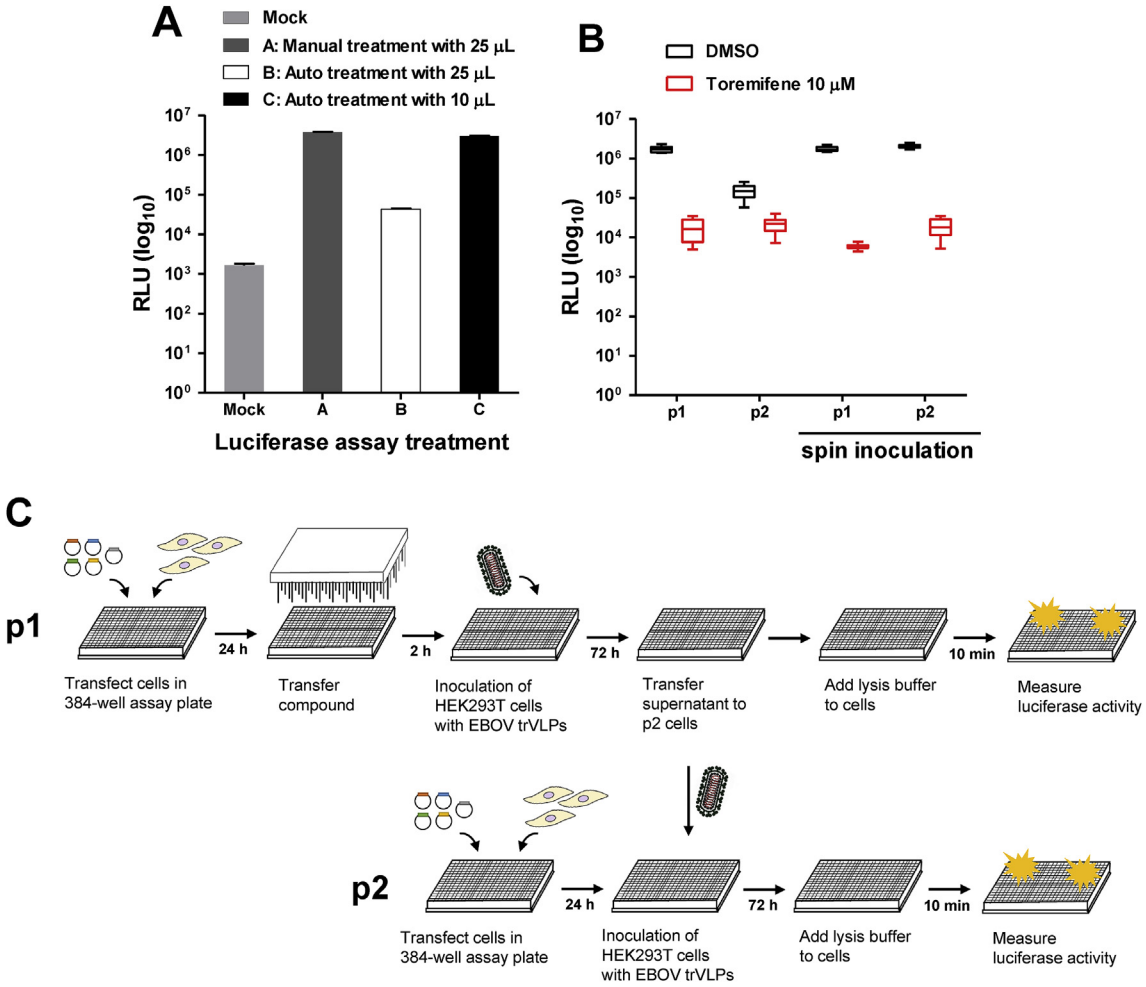

Fig. 2. EBOV trVLP HTS assay automation. (A) Adaptation to automated luciferase reagent dispensing. Comparison of manual reagent dispensing versus automated liquid handling at 72 h post-infection. (B) Supernatant transfer assay optimization. Spin inoculation was performed using centrifugation after supernatant was transferred from p1 to p2 cells. Infected cells treated with 0.5% DMSO (v/v) or 10 μM toremifene are shown in black and red box plots, respectively. (C) Optimized HTS assay schedule for EBOV trVLPs in 384-well microtiter plate. (For interpretation of the references to colour in this figure legend, the reader is referred to the Web version of this article.)

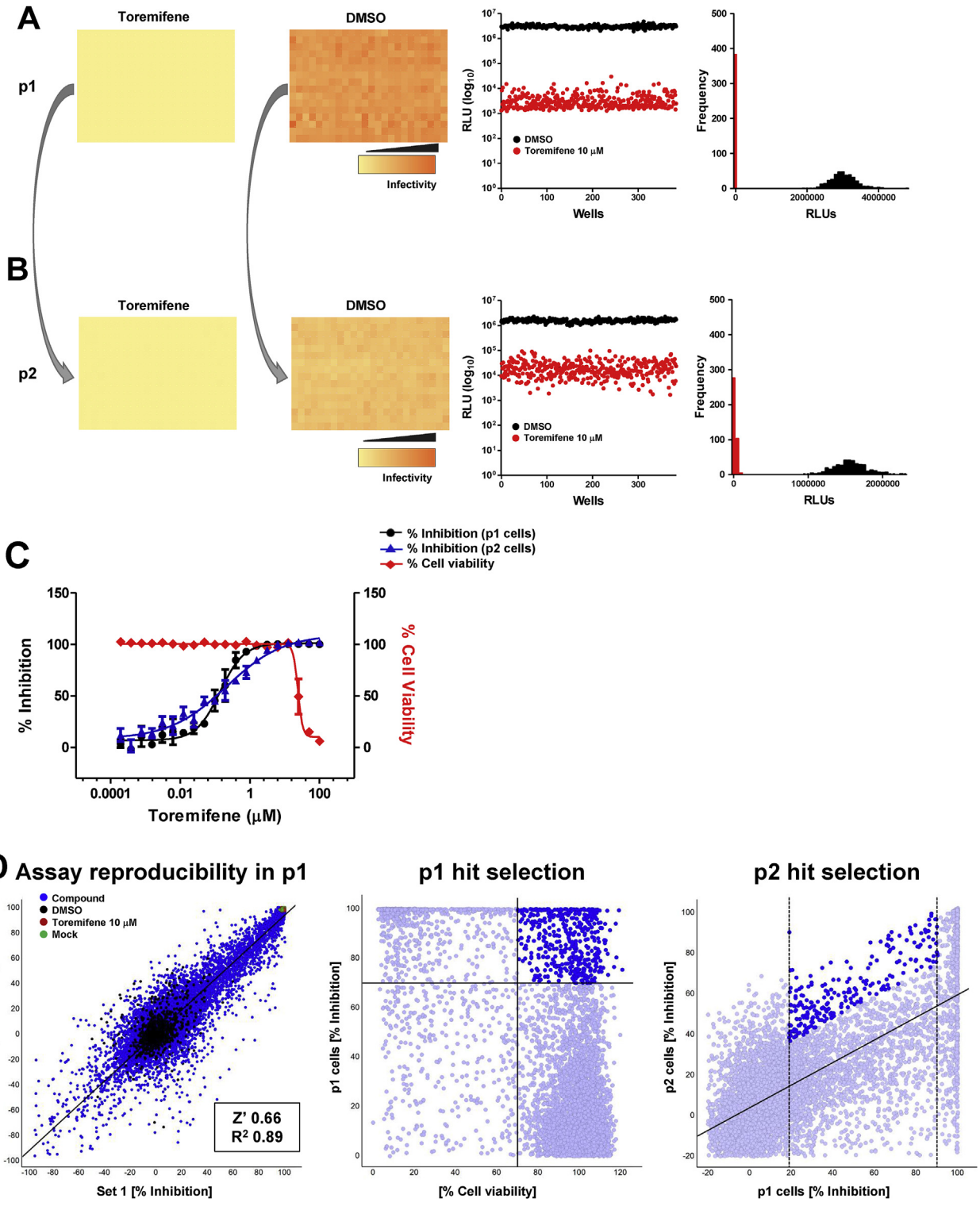

Fig. 3. EBOV trVLP HTS assay validation and compound screening. (A) Control run in p1 cells performed with an entire plate containing 0.5% DMSO (v/v) and 10 μM toremifene in 0.5% DMSO (v/v). Heat map analysis shows overall infectivity from high to low (orange to yellow). Scatter plot shows controls with 0.5% DMSO (v/v) (black) or toremifene (red); wells and resulting RLUs are depicted on the x- and y-axes, respectively. Histogram plot shows frequency on the y-axis and resulting RLUs on the x-axis. (B) Control run in p2 cells following the supernatant transfer step from previous p1 cells. (C) Reference DRC analysis with toremifene in HTS. Compound concentration, EBOV trVLP inhibition (%) in p1 and p2 cells, and cell viability (%) are depicted on the x-, left y- (black and blue), and right y-axes (red), respectively. (D) Scatter plot analysis in p1 cells in duplicate with controls and compounds (left). Compounds (blue), 0.5% DMSO (v/v) (black), toremifene 10 μM (red), non-infected cells, mock (green). Selection of 381 hits in p1 cells according to ≥70% EBOV trVLP inhibition of (y-axis) and ≥70% cell viability (x-axis) (middle). Linear regression revealed 49 hits selected in p2 cells (right).

Table 4
DRC analysis of tamoxifen and toremifene during the EBOV trVLP HTS campaign.

		Toremifene
p1 cells	EC_{50} (μM)	0.14 ± 0.05
	CC_{50} (μM)	26.96 ± 3.74
	Imax (%)	100
	TI	193
p2 cells	EC_{50} (μM)	0.18 ± 0.15

Values represent mean ± SD from 3 independent experiments.

increase the window of measurement, EBOV trVLPs were spin inoculated, which resulted in nearly 300- and 100-fold windows in p1 and p2 cells, respectively. Z′, S/B, and %CV values were calculated and are shown in Table 3. Spin inoculation was therefore incorporated in the HTS assay to achieve Z' > 0.5, increase the S/B ratio, and reduce the %CV. The EBOV trVLP HTS assay work flow is shown in Fig. 2C.

3.3. EBOV trVLP HTS assay validation, drug screening, and hit selection

Using the optimized and fully automated EBOV trVLP HTS assay conditions, we validated the assay by running controls in 384-well microtiter plates. Entire plates were treated with 0.5% DMSO (v/v) and toremifene at 10 μM in 0.5% DMSO (v/v) to monitor reproducibility and well-to-well variations. A heat map analysis of p1 cells demonstrated signal uniformity across the plate of DMSO and toremifene controls, with good separation of the controls (Fig. 3A). Luminescence was measured at $\sim 3 \times 10^6$ RLUs and $\sim 1 \times 10^3$ RLUs in cells treated with DMSO and toremifene, respectively, resulting in an S/B ratio of 3000 and Z′ of 0.63. After supernatant transfer to p2 cells, similar uniformity of signal was observed (Fig. 3B), whereas the total RLUs of DMSO were reduced by 2-fold to $\sim 1.5 \times 10^6$ RLUs and in toremifene-treated cells to $\sim 2 \times 10^4$ RLUs. The resulting S/B ratio of the controls in p2 with the EBOV trVLP system was acceptable at 20-fold. No systematic errors were observed, and the S/B ratio of 100 and Z' of 0.55 demonstrated that assay quality and performance were suitable for HTS.

After the successful HTS assay validation, we screened compound libraries consisting of a collection of 8354 small molecules containing bioactives with known targets (66%), FDA-approved drugs (28%), natural compounds (3%), and kinase inhibitors (3%). Compounds were screened in duplicates at a final concentration of 10 μM in 0.5% DMSO (v/v). For each replicate, two reference DRC plates containing EBOV inhibitor toremifene was included at a starting concentration of 100 μM in 0.5% DMSO (v/v) with 2-fold serial dilutions. EC_{50} and half-maximal cytotoxicity concentration (CC_{50}) value of reference compound was compared to previously reported data as a measure of assay robustness throughout the screen (Table 4). The EC_{50} values of toremifene in p1 and p2 cells were 0.14 μM and 0.18 μM, respectively, with an CC_{50} > 20 μM (Fig. 3C). Toremifene shows activity in p2 cells, because after inhibiting viral entry in p1 cells, fewer cells are infected which can replicate and secrete progeny virus. Consequently, after supernatant transfer from p1 to p2 cells this is reflected by a lower number of infectious particle leading to a reduced infection rate. These results demonstrated the assay's ability to identify inhibitors in the entire EBOV life cycle.

After screening 8,354 compounds, results of infected p1 cells were evaluated using a scatter plot analysis to monitor data point distribution (Fig. 3D, left). Replicate results in sets 1 and 2 were plotted to measure Z' and R^2 values of 0.66 and 0.89, respectively, reflecting high assay robustness and reproducibility. Controls performed as expected for 0.5% DMSO (v/v) and 10 μM toremifene at 0% and 100% inhibition, respectively. To select for entry and replication inhibitors, we utilized threshold selection criteria of ≥70% inhibition of EBOV trVLP reporter activity and ≥70% cell viability to nominate 381 compounds (Fig. 3D, middle). To select for morphogenesis and secretion inhibitors using the supernatant transfer strategy from p1 to p2 cells, we performed a linear regression analysis (Fig. 3D, right). A majority of compounds showed a correlation in activity between p1 and p2 cell % inhibition (fill line). Compounds below 20% inhibition in p1 were excluded due to background and those above 90% inhibition were excluded as potent (dash line). Next, compounds were selected with activity as morphogenesis and secretion inhibitors by the difference between p1 and p2 measurements. Finally, cytotoxic compounds were removed from the list and 49 compounds are selected as late-stage inhibitors. In total, 430 compounds were identified to inhibit EBOV trVLPs in p1 and p2 assays.

3.4. Hit confirmation

To confirm the antiviral activities of the 430 selected hits, compounds were supplied from internal library stocks and evaluated in the primary HTS assay by DRC analysis of serially diluted compounds. Besides calculating EC_{50} and CC_{50} values, and the resulting therapeutic index (TI), we also determined the Imax (%) as an additional criterion to prioritize hits. Of the selected compounds tested, 220 were confirmed in DRC analysis by applying a stringent hit confirmation criteria of TI ≥ 6 in p1 cells. These included 65 previously identified EBOV inhibitors and 1 confirmed in p2 cells. As a representative of the compounds confirmed by DRC analysis, 4 previously published EBOV inhibitors (Fig. 4A) and unpublished inhibitors (Fig. 4B) are shown. Additionally, the EC_{50} and CC_{50} values with their activities and pharmacologic actions are summarized in Table 5. Among the compounds selected for inhibiting EBOV in p2 cells (late steps including secretion), Bisacodyl showed no inhibitory activity in p1 cells (Fig. 4C), while p2 cell infection was dose-dependently inhibited with an EC_{50} of 1.89 μM and Imax of 73% (Table 6). This phenotype is characteristic for inhibitors interfering with late steps of the EBOV life cycle, like virion morphogenesis or egress. Furthermore, we confirmed the previously described EBOV entry inhibitors ML9, amodiaquine, sertraline, toremifene, bepridil and amiodarone and additionally identified five new drugs (iminodyn 17, nobiletin, ferroquine, N-Acetyl-L-leucyl-L-leucyl-L-methional, calpeptin) as shown in Table 7.

3.5. Hit triage and classification according to pharmacological actions

Among our confirmed hits, we selected two unpublished cathepsin L (CatL) inhibitors. N-Acetyl-L-leucyl-L-leucyl-L-methional, a highly potent inhibitor of CatL with lower inhibitory activity against cathepsin B (CatB), and calpeptin, which has been demonstrated to inhibit the CatL and cathepsin K were subjected to time-of-addition experiments to assess the antiviral activities during EBOV entry. Compounds were added to cells 16 h before or post-virus inoculation. Both CatL inhibitors showed exclusively anti-EBOV activity under the pretreatment condition (Fig. 5A), but only minor inhibition of infection was detected when the compounds were added 16 h post-virus inoculation (Fig. 5B). These results confirmed the antiviral activity of our newly identified CatL inhibitors during the early step of EBOV entry. EC_{50} and CC_{50} values from time-of-addition experiments are shown in Table 8. In contrast, cyanocobalamin, one of our newly identified inhibitors, showed similar antiviral activity under both time-of-addition assay conditions, indicating it functions after EBOV entry. Finally, the 220 confirmed hits were classified according to scaffold similarities and reported biological activities for further analysis. The pharmacological actions spanned 24 categories, with the most confirmed drugs in the area of

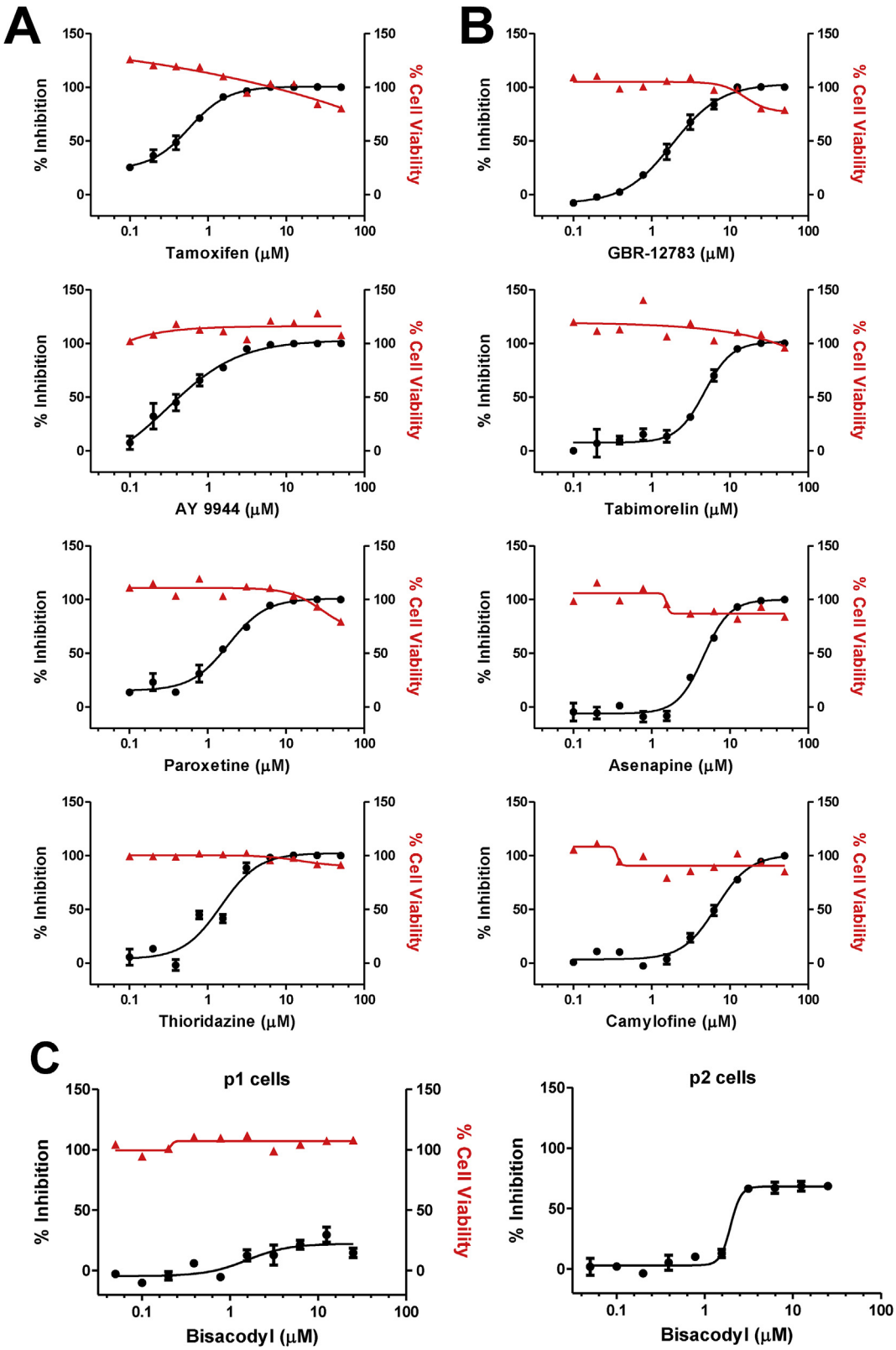

Fig. 4. Hit confirmation. (A) DRC analysis of published- and re-identified EBOV hits. (B) DRC analysis with unpublished hits. (C) DRC analysis of an inhibitor to block late life cycle steps.

Table 5
DRC analysis of previously published EBOV inhibitors and newly identified hits from the screen.

	Published				Unpublished			
	Tamoxifen	AY9944	Paroxetine	Thioridazine	GBR-12783	Tabimorelin	Asenapine	Camylofine
EC_{50} (μM)	0.58 ± 0.06	0.80 ± 0.16	1.83 ± 0.37	1.45 ± 0.26	1.91 ± 0.45	4.74 ± 0.03	4.59 ± 0.02	6.66 ± 0.47
CC_{50} (μM)	> 50	> 50	> 50	> 50	> 50	> 50	> 50	> 50
Imax (%)	100	100	100	100	100	100	100	100
TI	> 86	> 63	> 27	> 34	> 26	> 11	> 11	> 8
Pharmacologic action	Anticancer	N.D.	Anti-depressant	Anti-psychotic	Neurotrans- mitter agent	GPCR modulator	CNS agent	PNS agent

CNS: Central Nervous System, PNS: Peripheral Nervous System.
The mean ± SD of duplicate experiments are shown. Not determined (N.D.).

neurotransmitter- and central nervous system- (CNS) targeting therapeutics (Fig. 5C).

4. Discussion

Since EVD was discovered in 1976, EBOV outbreaks are reported on a nearly annual basis. The EBOV outbreak in 2014 with more than 11,000 casualties in West Africa (Baize et al., 2014), prompted governments to support research campaigns addressing unmet medical needs. This effort led to the development of the EBOV trVLP system, which allows for interrogation of the entire EBOV life cycle through entry, replication, and trVLP release under safe BSL2 conditions (Hoenen et al., 2006). The importance of this work has now been underscored by the occurrence in recent months of two outbreaks in the Democratic Republic of the Congo (http://www.who.int/ebola/en/).

In this report, we describe the utility of this system, the development of an HTS assay, and the results of screening 8354 compounds consisting of FDA-approved drugs and bioactives with known activities that can be quickly repurposed for therapeutic use and/or to study the mechanism of action to better understand the EBOV life cycle. The EBOV trVLP system is based on the transient transfection of six plasmids, which requires identifying suitable assay conditions to monitor viral entry, replication, and secretion. We evaluated various factors including cell numbers, transfection and inoculation procedures, and reference inhibitors to develop a robust 384-well plate assay. Toremifene and tamoxifen were selected as reference inhibitors and performed as previously reported using live virus, demonstrating that the trVLP system is a suitable tool to screen for drugs or targets (Johansen et al., 2015). After defining the HTS protocol, we validated the assay by infecting entire 384-well plates with EBOV trVLPs in the presence and absence of toremifene (EC_{100}) and demonstrated uniformity of infection by heat map analysis and calculated the S/B ratio of 850 and 74 in p1 and p2 cells, respectively. Compounds were subsequently screened at 10 μM in 0.5% DMSO (v/v) in duplicates. The HTS campaign was shown to be highly robust and reproducible as demonstrated by Z' and R^2 values of 0.66 and 0.89, respectively. Active compounds were selected by applying strict hit selection criteria of ≥70% EBOV replication inhibition and ≥70% cell viability to rule out those in which antiviral activity is influenced by cytotoxicity. This identified 381 and 49 hits in p1 and p2 cells, respectively. The nominated hits were supplied from internal library stocks, and 220 were confirmed in p1 and p2 cells by 10-point DRC analysis in the primary HTS assay. Among the confirmed hits, 174 compounds were classified as high priority with TI values of 6–331, and 65 compounds were previously published or patented as EBOV inhibitors using various cell culture systems.

Table 6
DRC analysis of Bisacodyl in p1 and p2 cells.

		Bisacodyl
p1 cells	EC_{50} (μM)	> 25
	CC_{50} (μM)	> 25
	Imax (%)	22
	TI	N.D.
p2 cells	EC_{50} (μM)	1.89 ± 0.24
	Imax (%)	73

The mean ± SD of duplicate experiments are shown. Not determined (N.D.).

As shown in Table 5, inhibitors tamoxifen, AY-9944, paroxetine maleate, and thioridazine were previously identified by using an EBOV VLP entry assays, with EC_{50} values in a comparable range to our results. This is suggesting that surrogate systems for EBOV entry using VLPs bearing the viral glycoproteins and the EBOV trVLP system exploit an identical entry mechanism and kinetics. Furthermore, CatB and CatL, both endosomal cysteine proteases, have been shown to be required for EBOV entry (Chandran et al., 2005). Both proteases are involved in the cleavage of EBOV GP1, which is an essential step in triggering fusion between the viral envelope and endosomal membrane and resulting in the release of the viral genome into the cytoplasm for replication. CatB and CatL are promising targets for anti-EBOV drugs and several inhibitors have been described.

In addition, we re-identified previously reported inhibitors like ML9, amodiaquine, sertraline, bepridil and amiodarone which are targeting described EBOV entry factors like myosin light chain kinase, CatB-dependent viral GP cleavage, and NPC1-dependent viral fusion. The remaining 109 high priority hits have not been reported yet and include inhibitors targeting different components of already described cellular restriction factors for EBOV entry such as the dynamin I and II GTPase inhibitor iminodyn 17, the endosomal acidification inhibitor ferroquine and CatL inhibitors N-Acetyl-L-leucyl-L-leucyl-L-methional and calpeptin. Similarly, the phosphoinositide-3 kinase-Akt pathway inhibitors demethylasterriquinone B1 and nobiletin were identified among the high-priority anti-EBOV hits. The identification of these potent inhibitors illustrate the sensitivity of our EBOV trVLP assay and confirm their corresponding specific cellular targets to be restrictive for EBOV entry using HIV-based VLPs pseudotyped with EBOV glycoproteins (Mulherkar et al., 2011; Saeed et al., 2008; Sun et al., 2017; Wool-Lewis and Bates, 1998; Zhou et al., 2016; Schornberg et al., 2006). Additionally, for phosphoinositide-3 kinase inhibition, we have newly identified 4 more anti-EBOV compounds interfering on different levels of the epidermal growth factor receptor (EGFR) signaling pathways. Furthermore, G-protein coupled receptors (GPCR) modulators identified in the screen include antagonists and agonists of histamine, dopamine, adrenergic and 5-HT (serotonin) receptors that were already published as cellular targets for EBOV entry (Cheng et al., 2015). We also identified several compounds targeting GPCRs like cannabinoid, κ-

Table 7
EBOV entry inhibitors previously reported and newly identified in the screen.

	ML9	Amodiaquine	Sertraline	Toremifene	Bepridil	Amiodarone	Iminodyn 17	Nobiletin	Ferroquine	N-Acetyl-L-leucyl-L- leucyl-L-methional	Calpeptin
EC_{50} (μM)	1.57 ± 0.07	2.17 ± 0.27	2.34 ± 0.86	0.29 ± 0.05	2.90 ± 0.09	1.83 ± 0.04	8.52 ± 1.68	0.69 ± 0.13	0.59 ± 0.02	0.57 ± 0.27	0.51 ± 0.07
CC_{50} (μM)	> 50	> 50	> 50	> 50	> 50	> 50	> 50	> 50	7.88	> 50	> 50
Imax (%)	100	100	100	100	100	100	79	89	100	100	97
TI	> 32	> 23	> 21	> 172	> 17	> 27	> 6	> 72	13	> 88	> 98
Inhibitor published (PMID)	*In vitro* No EC_{50} (21907381)	*In vitro* EC_{50} 3.8 μM (26310922)	*In vitro* EC_{50} 3.3 μM (26041706)	*In vitro* EC_{50} 0.6 μM (27890675)	*In vitro* EC_{50} 5.1 μM (26041706)	*In vitro*EC_{50} 5.6 μM (25933611)	No	No	No	No	No
Drug current Application	N.D.	Anti-malarial	Anti-depressant	Anti-cancer	Anti-angina	Anti-arrhythmic	N.D.	N.D.	Anti-malarial	N.D.	N.D.
Proposed Mechanism of Action (PMID)	Myosin light chain kinase	CatB dependent viral GP cleavage	NPC1-dependent viral fusion	Viral fusion	NPC1-dependent viral fusion	NPC1-dependent viral fusion	Dynamin-dependent viral endocytosis (21907381)	PI3K-Akt pathway dependent vesicular/viral trafficking (18769720)	Endosomal pH dependent viral fusion (27890675)	Cat L dependent viral GP cleavage (16571833)	CatL-dependent viral GP cleavage (16571833)

The mean ± SD of duplicate experiments are shown. Not determined (N.D.).

opioid, δ-opioid, nociceptin opioid peptide (NOP), and neurokinin 1 receptors. Together with other kinase inhibitors, these compounds are represented in the pharmacological group of protein and cellular kinase inhibitors (Fig. 5C) that were described having a broad-spectrum antiviral activity for hemorrhagic fever viruses like EBOV (Mohr et al., 2015).

In addition to the reported EBOV entry inhibitors, we re-identified several previously published EBOV RNA synthesis inhibitors in p1 cells, such as azacitidine, gedunin, mycophenolic acid, and cycloheximide (Edwards et al., 2015). Time-of-addition assays revealed that our cathepsin L inhibitors act exclusively in viral entry during the first 16 h post-infection, whereas the newly identified cyanocobalamin also showed strong inhibition after the establishment of infection and therefore is most likely active in an EBOV life cycle step like replication (Fig. 5A and B). Important to note, bisacodyl is to our knowledge the first reported inhibitor to specifically interfere with EBOV morphogenesis and egress which does not belong to the class of quinoxaline-based inhibitors (Loughran et al., 2016). Collectively, our data demonstrate that the EBOV trVLP system is suitable for identifying novel inhibitors targeting viral entry, replication, as well as morphogenesis and egress. The re-identification of previously described EBOV entry and replication inhibitors suggests that the trVLP entry mechanism is comparable to other used surrogates and the authentic EBOV system and confirms the authenticity of EBOV trVLP entry in p1 cell infection.

In conclusion, we screened FDA-approved drugs and biological actives using the EBOV trVLP system and identified 220 compounds that efficiently inhibit various stages of the viral life cycle. Several of these drugs have already been used for EBOV treatments, such as amodiaquine, which is a cationic amphiphilic drug (CAD) similar in structure to chloroquine, a previously described EBOV entry inhibitor. During the 2014 EBOV outbreak, the treatment of selected malaria patients in Liberia were switched from antimalarial containing lumefantrine to one containing amodiaquine and noted a significant decrease in case fatality rates in Ebola treatment centers. Furthermore, the anti-arrhythmic drug amiodarone, also a CAD, was tested in clinical trials in 65 patients at up to 20 mg/kg/day during the 2014 EBOV outbreak in Freetown, Sierra Leone. The reported case fatality rate was 40% compared with 50% for the entire patient population (http://www.who.int/medicines/ebola-treatment/2015_0703TablesofEbolaDrugs.pdf). As mentioned by the WHO, it cannot be excluded that decreasing fatalities were due to lesser toxicity of amodiaquine compared to artemether-lumefantrine and it is not known whether the effect described in patients treated with amiodarone is significant. However, while further investigations on a potential anti-EBOV activity of amodiaquine and amiodarone in animals are needed, our and others *in vitro* results are indicating that an antiviral activity of the compounds may have been responsible for the effects observed in EBOV patients. Drug repurposing strategies can be suitable to identify effective, affordable, and accessible EVD therapies and *in vitro* screening campaigns are powerful tools to identify drug candidates. Currently, we are evaluating several confirmed hits in a collaborative study using authentic EBOV in BSL4 containment to quickly repurpose favorable FDA-approved drugs as urgently needed EVD treatments.

Conflicts of interest

All authors declare that they have no conflict of interest.

Author contributions

NL, HK, JH, SM, JL, YK and IC performed the experiments; HL and CR contributed to compound management; DS, JYM, TH and MPW conceived the project; NL, DS, AK and MPW analyzed the data and wrote the manuscript.

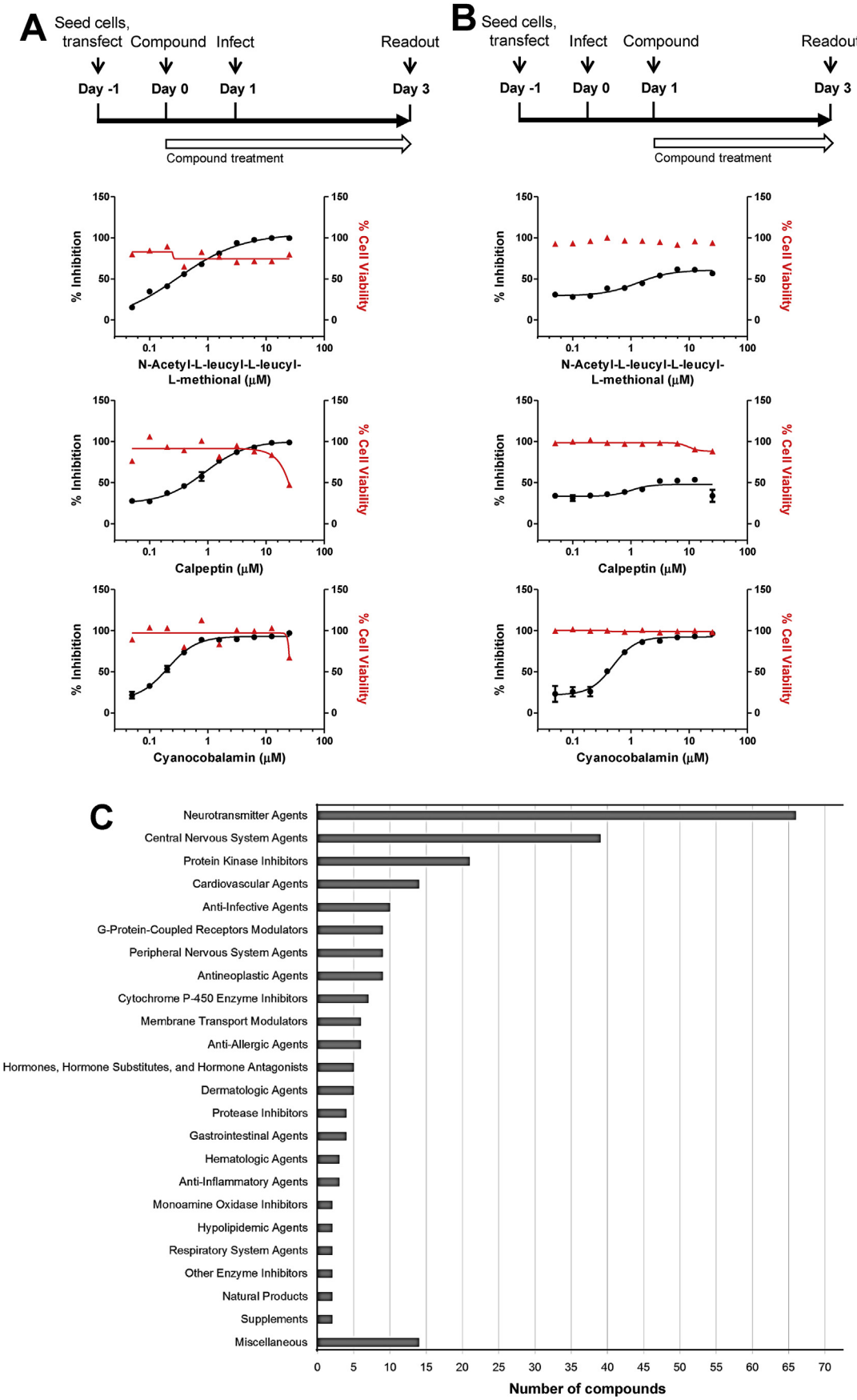

Fig. 5. Hit triage and grouping according to pharmacological actions. Time-of-addition experiments. (A) Compound treatment 16 h before virus inoculation. (B) Compound treatment 16 h after virus inoculation. DRC analysis was performed as described before. (C) Pharmacological action profiling of inhibitors. We clustered 220 confirmed compounds based on scaffold analysis from MeSH (National Library of Medicine - Medical Subject Headings), ChemIDplus, and SciFinder databases. The horizontal bar graph (dark grey) shows the number of compounds on the x-axis and representative 24 pharmacological action categories on the y-axis.

Table 8
DRC analysis of N-Acetyl-L-leucyl-L-leucyl-L-methional, calpeptin, and cyanocobalamin in the time-of-addition experiments.

		N-Acetyl-L-leucyl-L-leucyl-L-methional	Calpeptin	Cyanocobalamin
Treatment of compounds 16 h before virus inoculation	EC_{50} (μM)	0.31 ± 0.24	0.66 ± 0.23	0.21 ± 0.01
	CC_{50} (μM)	> 25	> 25	> 25
	Imax (%)	105	101	93
	TI	81	38	119
Treatment of compounds 16 h post virus inoculation	EC_{50} (μM)	N.D.	N.D.	0.50 ± 0.06
	CC_{50} (μM)	> 25	> 25	> 25
	Imax (%)	61	48	92
	TI	N.D.	N.D.	50

The mean ± SD of duplicate experiments are shown. Not determined (N.D.).

Acknowledgments

Funding: This work was supported by the Institut Pasteur Ebola Task Force and a National Research Foundation of Korea (NRF) grant funded by the Korea government (MSIT) (NRF-2017M3A9G6068246), Gyeonggi-do.

References

Anantpadma, M., Kouznetsova, J., Wang, H., Huang, R., Kolokoltsov, A., Guha, R., Lindstrom, A.,R., Shtanko, O., Simeonov, A., Maloney, D.J., Maury, W., LaCount, D.J., Jadhav, A., Davey, R.A., 2016. Large-scale screening and identification of novel ebola virus and marburg virus entry inhibitors. Antimicrob. Agents Chemother. 60, 4471–4481.

Baize, S., Pannetier, D., Oestereich, L., Rieger, T., Koivogui, L., Magassouba, N., Soropogui, B., Sow, M.S., Keita, S., De Clerck, H., Tiffany, A., Dominguez, G., Loua, M., Traore, A., Kolie, M., Malano, E.R., Heleze, E., Bocquin, A., Mely, S., Raoul, H., Caro, V., Cadar, D., Gabriel, M., Pahlmann, M., Tappe, D., Schmidt-Chanasit, J., Impouma, B., Diallo, A.K., Formenty, P., Van Herp, M., Gunther, S., 2014. Emergence of zaire ebola virus disease in Guinea. N. Engl. J. Med. 371, 1418–1425.

Basu, A., Mills, D.M., Mitchell, D., Ndungo, E., Williams, J.D., Herbert, A.S., Dye, J.M., Moir, D.T., Chandran, K., Patterson, J.L., Rong, L., Bowlin, T.L., 2015. Novel small molecule entry inhibitors of ebola virus. J. Infect. Dis. 212, S425–S434.

Bemis, G.W., Murcko, M.A., 1996. The properties of known drugs. 1. Molecular frameworks. J. Med. Chem. 39, 2887–2893.

Chandran, K., Sullivan, N.J., Felbor, U., Whelan, S.P., Cunningham, J.M., 2005. Endosomal proteolysis of the Ebola virus glycoprotein is necessary for infection. Science 308, 1643–1645.

ChemIDPlus database, National Library of Medicine, 2017. https://chem.nlm.nih.gov/chemidplus/.

Cheng, H., Lear-Rooney, C.M., Johansen, L., Varhegyi, E., Chen, Z.W., Olinger, G.G., Rong, L., 2015. Inhibition of ebola and marburg virus entry by G Protein-coupled receptor antagonists. J. Virol. 89, 9932–9938.

Dyall, J., Nelson, E.A., DeWald, L.E., Guha, R., Hart, B.J., Zhou, H., Postnikova, E., Logue, J., Vargas, W.M., Gross, R., Michelotti, J., Deiuliis, N., Bennett, R.S., Crozier, I., Holbrook, M.R., Morris, P.J., Klumpp-Thomas, C., McKnight, C., Mierzwa, T., Shinn, P., Glass, P.J., Johansen, L.M., Jahrling, P.B., Hensley, L.E., Olinger Jr., G.G., Thomas, C., White, J.M., 2018. Identification of combinations of approved drugs with synergistic activity against ebola virus in cell cultures. J. Infect. Dis. https://doi.org/10.1093/infdis/jiy304.

Edwards, M.R., Pietzsch, C., Vausselin, T., Shaw, M.L., Bukreyev, A., Basler, C.F., 2015. High-throughput minigenome system for identifying small-molecule inhibitors of ebola virus replication. ACS Infect. Dis. 1, 380–387.

Hoenen, T., Groseth, A., Kolesnikova, L., Theriault, S., Ebihara, H., Hartlieb, B., Bamberg, S., Feldmann, H., Ströher, U., Becker, S., 2006. Infection of naive target cells with virus-like particles: implications for the function of ebola virus VP24. J. Virol. 80, 7260–7264.

Hoenen, T., Feldmann, H., 2014. Reverse genetics systems as tools for the development of novel therapies against filoviruses. Expert Rev. Anti-infect. Ther. 12, 1253–1263.

Johansen, L.M., Brannan, J.M., Delos, S.E., Shoemaker, C.J., Stossel, A., Lear, C., Hoffstrom, B.G., Dewald, L.E., Schornberg, K.L., Scully, C., Lehár, J., Hensley, L.E., White, J.M., Olinger, G.G., 2013. FDA-approved selective estrogen receptor modulators inhibit Ebola virus infection. Sci. Transl. Med. 5 190ra79.

Johansen, L.M., DeWald, L.E., Shoemaker, C.J., Hoffstrom, B.G., Lear-Rooney, C.M., Stossel, A., Nelson, E., Delos, S.E., Simmons, J.A., Grenier, J.M., Pierce, L.T., Pajouhesh, H., Lehár, J., Hensley, L.E., Glass, P.J., White, J.M., Olinger, G.G., 2015. A screen of approved drugs and molecular probes identifies therapeutics with anti-Ebola virus activity. Sci. Transl. Med. 7 290ra89.

Kouznetsova, J., Sun, W., Martínez-Romero, C., Tawa, G., Shinn, P., Chen, C.Z., Schimmer, A., Sanderson, P., McKew, J.C., Zheng, W., García-Sastre, A., 2014. Identification of 53 compounds that block Ebola virus-like particle entry via a repurposing screen of approved drugs. Emerg. Microb. Infect. 3, e84.

Law, V., Knox, C., Djoumbou, Y., Jewison, T., Guo, A.C., Liu, Y., Maciejewski, A., Arndt, D., Wilson, M., Neveu, V., Tang, A., Gabriel, G., Ly, C., Adamjee, S., Dame, Z.T., Han, B., Zhou, Y., Wishart, D.S., 2014. DrugBank 4.0: shedding new light on drug metabolism. Nucleic Acids Res. 42, 1091–1097.

Loughran, H.M., Han, Z., Wrobel, J.E., Decker, S.E., Ruthel, G., Freedman, B.D., Harty, R.N., Reitz, A.B., 2016. Quinoxaline-based inhibitors of ebola and marburg VP40 egress. Bioorg. Med. Chem. Lett 26, 3429–3435.

MESH database, National Library of Medicine, 2017. http://www.nlm.nih.gov/mesh/MBrowser.html.

Mohr, E.L., McMullan, L.K., Lo, M.K., Spengler, J.R., Bergeron, É., Albariño, C.G., Shrivastava-Ranjan, P., Chiang, C.F., Nichol, S.T., Spiropoulou, C.F., Flint, M., 2015. Inhibitors of cellular kinases with broad-spectrum antiviral activity for hemorrhagic fever viruses. Antivir. Res. 120, 40–47.

Mulherkar, N., Raaben, M., de la Torre, J.C., Whelan, S.P., Chandran, K., 2011. The Ebola virus glycoprotein mediates entry via a non-classical dynamin-dependent macropinocytic pathway. Virology 419, 72–83.

Nelson, E.A., Barnes, A.B., Wiehle, R.D., Fontenot, G.K., Hoenen, T., White, J.M., 2016. Clomiphene and its isomers block ebola virus particle entry and infection with similar potency: potential therapeutic implications. Viruses 8, E206.

Nelson, E.A., Dyall, J., Hoenen, T., Barnes, A.B., Zhou, H., Liang, J.Y., Michelotti, J., Dewey, W.H., DeWald, L.E., Bennett, R.S., Morris, P.J., Guha, R., Klumpp-Thomas, C., McKnight, C., Chen, Y.C., Xu, X., Wang, A., Hughes, E., Martin, S., Thomas, C., Jahrling, P.B., Hensley, L.E., Olinger Jr., G.G., White, J.M., 2017. The phosphatidylinositol-3-phosphate 5-kinase inhibitor apilimod blocks filoviral entry and infection. PLoS Neglected Trop. Dis. 11, e0005540.

Saeed, M.F., Kolokoltsov, A.A., Freiberg, A.N., Holbrook, M.R., Davey, R.A., 2008. Phosphoinositide-3 kinase-Akt pathway controls cellular entry of Ebola virus. PLoS Pathog. 4, e1000141.

Schornberg, K., Matsuyama, S., Kabsch, K., Delos, S., Bouton, A., White, J., 2006. Role of endosomal cathepsins in entry mediated by the Ebola virus glycoprotein. J. Virol. 80, 4174–4178.

SciFinder, Chemical Abstract Services, 2017. https://scifinder.cas.org/scifinder.

Sun, W., He, S., Martínez-Romero, C., Kouznetsova, J., Tawa, G., Xu, M., Shinn, P., Fisher, E., Long, Y., Motabar, O., Yang, S., Sanderson, P.E., Williamson, P.R., García-Sastre, A., Qiu, X., Zheng, W., 2017. Synergistic drug combination effectively blocks Ebola virus infection. Antivir. Res. 137, 165–172.

Watt, A., Moukambi, F., Banadyga, L., Groseth, A., Callison, J., Herwig, A., Ebihara, H., Feldmann, H., Hoenen, T., 2014. A novel life cycle modeling system for Ebola virus shows a genome length-dependent role of VP24 in virus infectivity. J. Virol. 88, 10511–10524.

Wool-Lewis, R.J., Bates, P., 1998. Characterization of Ebola virus entry by using pseudotyped viruses: identification of receptor-deficient cell lines. J. Virol. 72, 3155–3160.

Zhang, J.H., Chung, T.D., Oldenburg, K.R., 1999. A simple statistical parameter for use in evaluation and validation of high throughput screening assays. J. Biomol. Screen 4, 67–73.

Zhou, N., Pan, T., Zhang, J., Li, Q., Zhang, X., Bai, C., Huang, F., Peng, T., Zhang, J., Liu, C., Tao, L., Zhang, H., 2016. Glycopeptide antibiotics potently inhibit cathepsin L in the late endosome/lysosome and block the entry of ebola virus, Middle East respiratory syndrome coronavirus (MERS-CoV), and severe acute respiratory syndrome coronavirus (SARS-CoV). J. Biol. Chem. 291, 9218–9232.